Supporting Information

1 COMPUTATIONAL DETAILS

The first-principles calculations are based on density functional theory (DFT) methods using the Vienna *Ab initio* Simulation Package (VASP)[1, 2]. The Perdew-Burke-Ernzerhof (PBE) functional of generalized gradient approximation (GGA) [3] is adopted for the exchange-correlation interactions, with the Hubbard term correction of U = 3.0 eV on the d-orbital of Ti to describe the strongly correlated interactions of transition metal elements. The residual force and energy convergence tolerances are set to 10^{-3} eV/Å and 10^{-6} eV, respectively. The plane-wave cutoff is set to 500 eV. The Brillouin zone is sampled with a Γ-centered k-point mesh of 12×12×1. The phonon spectrum is calculated using density functional perturbation theory (DFPT) as implemented in the PHONOPY code [4]. The edge states and Berry curvature were calculated in the tight-binding models constructed using the Wannier representation as implemented in the WANNIER90 [5] and WannierTools packages [6].

2 TOTAL-ENERGY MAPPING METHOD

To evaluate the magnetic exchange parameters of the four monolayers studied, a Heisenberg model is built. The Hamiltonian is written as

$$H_0 = -J_1 \sum_{\langle i,j \rangle} \boldsymbol{S_i} \cdot \boldsymbol{S_j} - J_2 \sum_{\langle\langle i,j \rangle\rangle} \boldsymbol{S_i} \cdot \boldsymbol{S_j} \tag{S1}$$

where $\langle i,j\rangle/\langle\langle i,j\rangle\rangle$ represents the NN/NNN spins between the sites i and j, J_1/J_2 denotes the NN/NNN exchange value, S_i represents the magnetic moment at site i. Here, $|\boldsymbol{S}| = 1$ and the total energies of the materials with the FM, AFM-s, and AFM-z magnetic structures are H_{FM}, $H_{\mathrm{AFM-s}}$ and $H_{\mathrm{AFM-z}}$. The J_1 and J_2 can be calculated with following equations:

$$H_{\mathrm{FM}} = -6J_1S^2 - 12J_2S^2 + E_0 \tag{S2}$$

$$H_{\mathrm{AFM-s}} = 2J_1S^2 + 4J_2S^2 + E_0 \tag{S3}$$

$$H_{\mathrm{AFM-z}} = -2J_1S^2 + 4J_2S^2 + E_0 \tag{S4}$$

where E_0 is the ground-state energy independent of the spin configuration. The calculated results of J_1 and J_2 are listed in Table 1.

Table S1 Calculated relative energy (ΔE) of FM, AFM-n, AFM-z, and AFM-s for Ti_2X_2 (X = P, As, Sb, Bi), where their energy of FM was normalized to 0 meV.

ΔE/meV	FM	AFM-n	AFM-z	AFM-s
Ti_2P_2	Ground State	680.54	257.27	473.65
Ti_2As_2	Ground State	632.04	237.41	557.07
Ti_2Sb_2	Ground State	822.51	228.74	623.24
Ti_2Bi_2	Ground State	1306.15	125.10	525.16

3 LOW-ENERGY EFFECTIVE HAMILTONIAN OF DIRAC FERMIONS

3.1 The case of Ti_2X_2 (X = P, As)

The electronic Bloch states of monolayer Ti_2X_2 (X = P, As) near the Fermi level are mainly contributed by the spin-up $d_{x^2-y^2}$ and d_{xz} orbitals of Ti atoms. When the SOC is excluded, six equivalent degenerate points appear in the first Brillouin zone. Let us consider the degenerate point along Γ-K. Symmetry generators of the little group for generic k points along Γ-K include E and C_{2x}. Character table of irreducible representations along Γ-K is displayed in Table S2. Valence and conduction bands around the Fermi level belong to the irreducible representation Δ1 and Δ2, respectively.

Table S2 Character table of the little group for generic k points along Γ-K.

	E	C_{2x}
Δ1	1	1
Δ2	1	-1

Under the two bases of valence and conduction bands, $C_{2x} = \sigma_x$, where the Pauli matrices σ act on the orbital space. Therefore, a 2×2 $\boldsymbol{k}\cdot\boldsymbol{p}$ effective Hamiltonian is constructed for k points along Γ-K:

$$H_{\text{eff}} = A(k)\sigma_x + B(k)\sigma_z + C(k)\sigma_0 \tag{S5}$$

where $A(k) = A_1 k_y + A_2 k_x k_y$, $B(k) = C_0 + C_1 k_x + C_2 k_x^2 + C_3 k_y^2$, $C(k) = D_0 + D_1 k_x + D_2 k_x^2 + D_3 k_y^2$. By considering the first-order term, the two bands cross in conditions of $A(k) = 0$ and $B(k) = 0$, giving degenerate points ($\pm k_D$, 0). Near the degenerate point (k_D, 0), the effective Hamiltonian can be expressed as $H_{\text{eff}}(q_x, q_y) = Aq_y\sigma_x + Bq_x\sigma_z + Cq_x\sigma_0$, where $q_x = k_x - k_D$, $q_y = k_y$. Through a basis transformation in the orbital space, we get $H_{\text{eff}}(q_x, q_y) = Aq_x\sigma_x' + Bq_y\sigma_y' + Cq_x\sigma_0'$.

The spin-orbit coupling Hamiltonian $L\cdot S$ in the $|d_{x^2-y^2\uparrow}\rangle$, $|d_{x^2-y^2\downarrow}\rangle$, $|d_{xz\uparrow}\rangle$ and $|d_{xz\downarrow}\rangle$ representations is

$$L\cdot S = \begin{pmatrix} 0 & is_y \\ -is_y & 0 \end{pmatrix} \tag{S6}$$

This is using the z-axis as the quantization axis. If any axis (θ, φ) is used as the quantization axis, we need perform a transformation,

$$U = I_{2\times 2} \otimes \begin{pmatrix} cos\frac{\theta}{2} & -sin\frac{\theta}{2} \\ e^{i\varphi}sin\frac{\theta}{2} & e^{i\varphi}\sin\frac{\theta}{2} \end{pmatrix} \tag{S7}$$

and the Hamiltonian $L\cdot S$ is transformed into

$$H' = U^{\dagger}L\cdot SU = \begin{pmatrix} 0 & 0 & i\sin\varphi\sin\theta & e^{i\varphi}\cos^2\frac{\theta}{2} + e^{-i\varphi}\sin^2\frac{\theta}{2} \\ 0 & -e^{i\varphi}sin^2\frac{\theta}{2} - e^{-i\varphi}\cos^2\frac{\theta}{2} & -i\sin\varphi\sin\theta & \\ & 0 & 0 & \\ \dagger & & 0 & \end{pmatrix} \tag{S8}$$

When the magnetization direction lies in the x-y plane ($\theta = 90°$), and the electron states near the Fermi level are predominantly occupied by a single spin channel. Consequently, the effective Hamiltonian $L\cdot S$ in the $|d_{x^2-y^2\rightarrow}\rangle$ and $|d_{xz\rightarrow}\rangle$ representations is

$$H' = \begin{pmatrix} 0 & i\sin\varphi \\ -i\sin\varphi & 0 \end{pmatrix} = M\sigma_y = M\sigma_z' \tag{S9}$$

So, when φ is not equal to 0°and 180°, a mass term will be introduced into the original Hamiltonian, leading to the formation of a Dirac gap.

3.2 The case of Ti_2X_2 (X = Sb, Bi)

The electronic Bloch states of monolayer Ti_2X_2 (X = Sb, Bi) near the Fermi level are mainly contributed by the spin-up d_{yz} and d_{xz} orbitals of Ti atoms. When the SOC is excluded, two Dirac points appear at K and K′ points. Let us consider the degenerate point at K. Symmetry generators of the little group for K points include E, C_{2x} and C_{3z}. Character table of irreducible representations at K is displayed in Table S3. The degenerate point around the Fermi level belongs to the irreducible representation K_3.

Table S3 Character table of the little group for K points.

	E	C_{2x}	C_{3z}
K_1	1	1	1
K_2	1	-1	1
K_3	2	0	-1

Under the two bases of d_{xz} and d_{yz} orbitals, $C_{2x} = \sigma_z$ and $C_{3z} = \frac{\sigma_0}{2} + i\frac{\sqrt{3}}{2}\sigma_y$. Therefore, a 2×2 $\boldsymbol{k}\cdot\boldsymbol{p}$ effective Hamiltonian is constructed for K points:

$$H_{\text{eff}} = A(k)\sigma_z + B(k)\sigma_x + C(k)\sigma_0 \tag{S10}$$

where $A(k) = A_1 k_x + A(k_x^2 - k_y^2)$, $B(k) = A_1 k_y - 2A_2 k_x k_y$, $C(k) = C_0 + C_0(k_x^2 + k_y^2)$. By considering the first-order term and the condition of $C(k) = 0$, the effective Hamiltonian can be represented as $H_{\text{eff}} = A_1 k_x \sigma_z + A_1 k_y \sigma_x = A_1 k_x \sigma_x' + A_1 k_y \sigma_y'$.

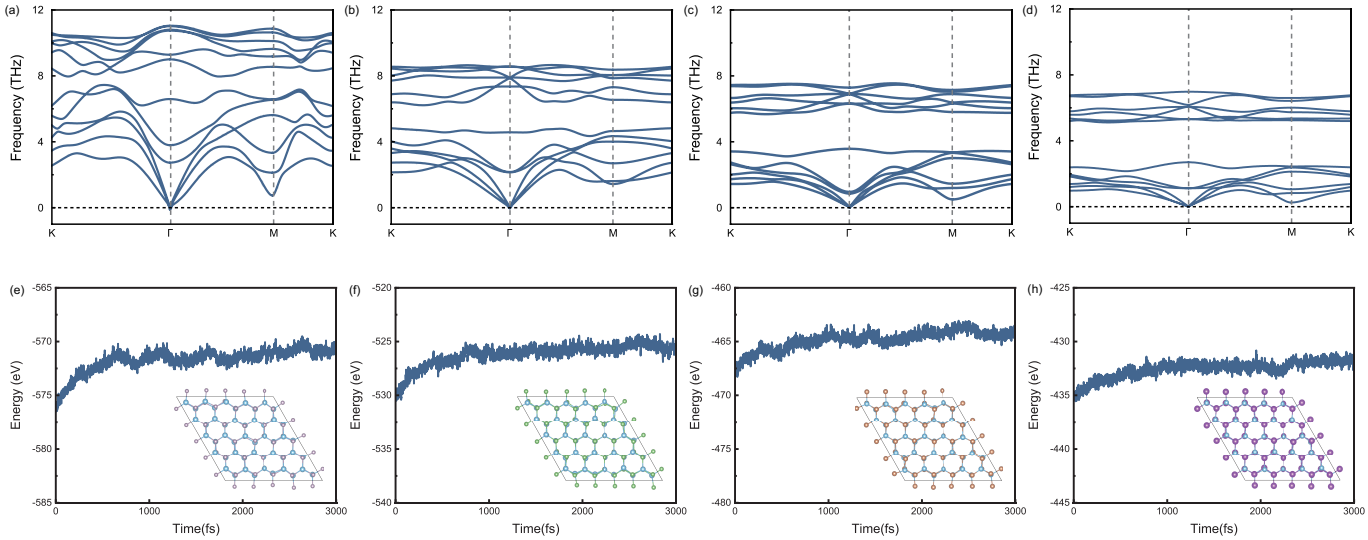

Fig. S1 **(a)-(d)** Calculated phonon spectra for Ti_2P_2, Ti_2As_2, Ti_2Sb_2 and Ti_2Bi_2, respectively. **(e)-(h)** Total energy fluctuations of the monolayers Ti_2P_2, Ti_2As_2, Ti_2Sb_2 and Ti_2Bi_2, respectively, during 3 ps MD simulation at 300 K. The final structures after MD simulation are shown in the insets.

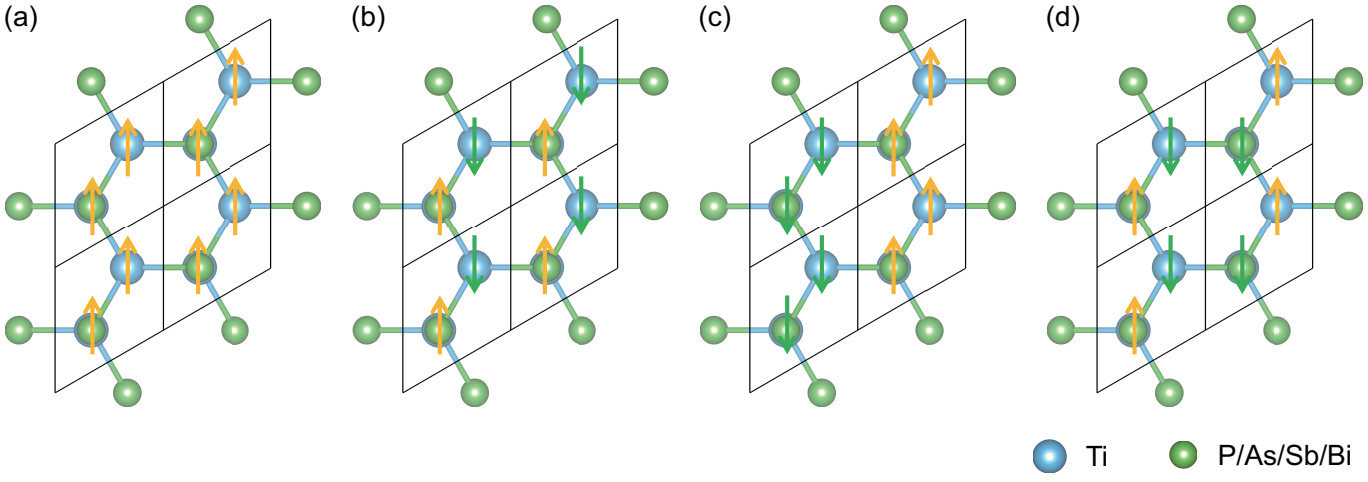

Fig. S2 **(a)-(d)** Schematics of the four possible magnetic configurations: FM, AFM-n, AFM-z, and AFM-s. Their energy is listed in Table S1.

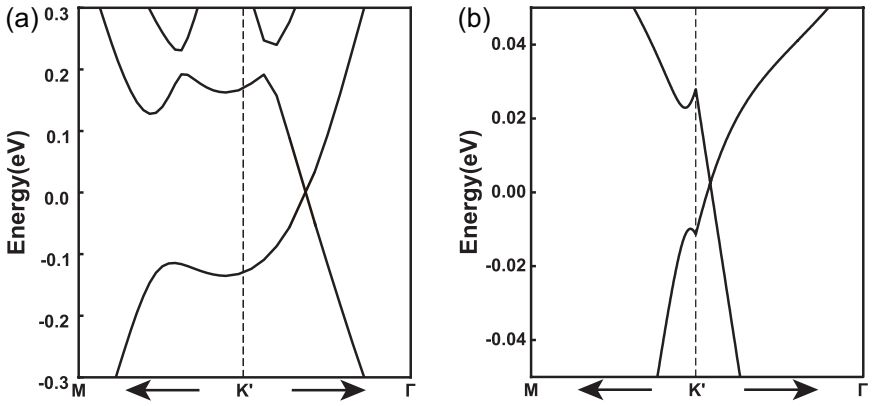

Fig. S3 Bulk band structure of monolayer **(a)** Ti_2As_2 and **(b)** Ti_2Sb_2 along high symmetry line M-K′-Γ in the presence of SOC and magnetization lying in the *x*-direction. They both have an intersection along the K′-Γ path.

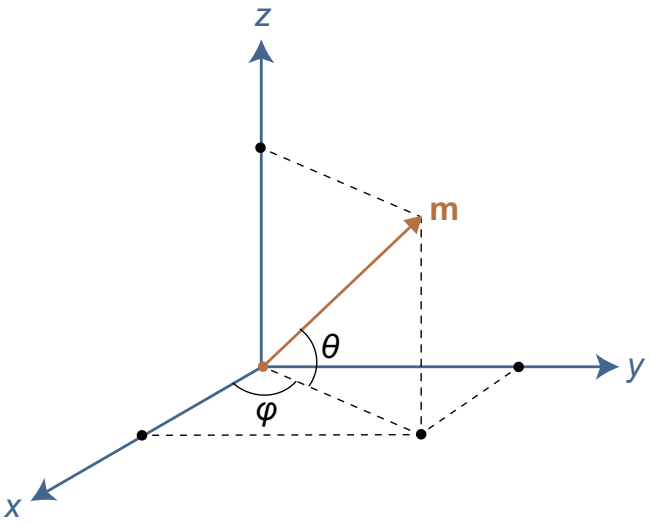

Fig. S4 Definition of magnetization direction azimuthal angle φ and polar angle θ.

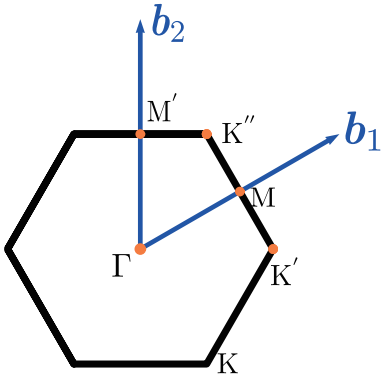

Fig. S5 First Brillouin zone with marked high symmetry points Γ, K, K′, K″, M, M′. $\boldsymbol{b}_1$ and $\boldsymbol{b}_2$ are reciprocal lattice vectors.

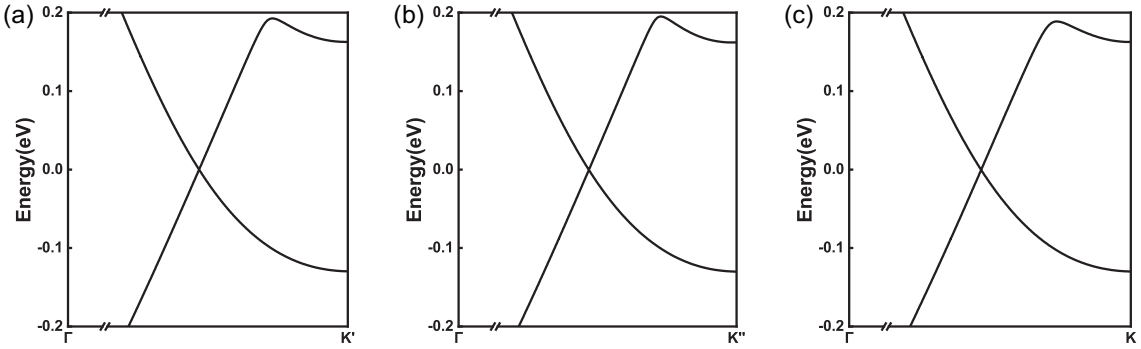

Fig. S6 Band structures of the Ti_2As_2 along high symmetry line Γ-K (K′, K″) considering SOC with magnetization lying in *x*-*y* plane with **(a)** $\varphi = 0°(180°)$, **(b)** $\varphi = 60°(210°)$, **(c)** $\varphi = 120°(300°)$.

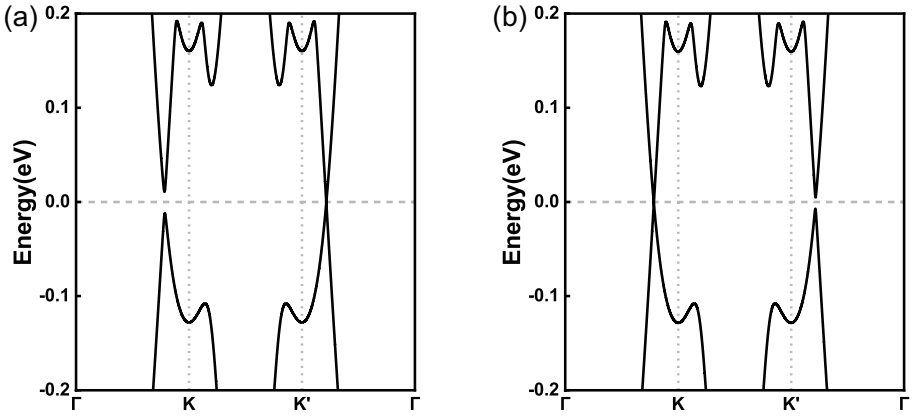

Fig. S7 Band structures of the Ti_2As_2 along high symmetry line Γ-K-K′-Γ considering SOC with magnetization lying in *x*-*z* plane with **(a)** $\theta = 85.6°(265.6°)$, **(b)** $\theta = 98.6°(278.6°)$.

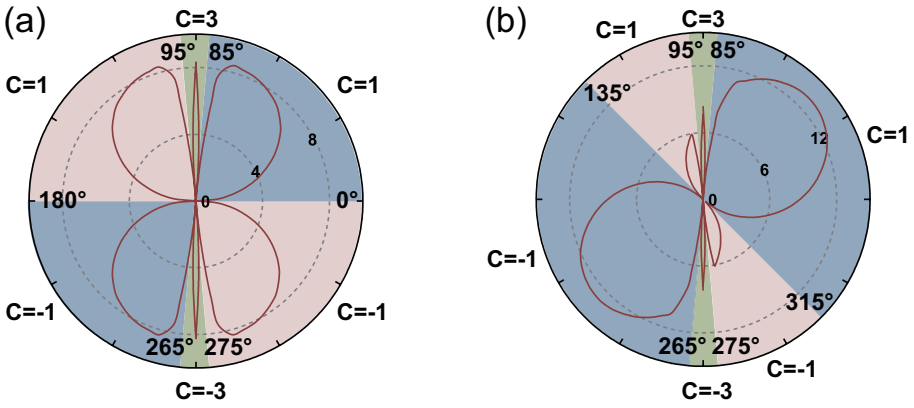

Fig. S8 For Ti_2As_2, Phase diagram of Chern number as a function of polar angle θ for the out-of-plane magnetization along different **(a)** $\varphi = 0°$ and **(b)** $\varphi = 5°$ path.

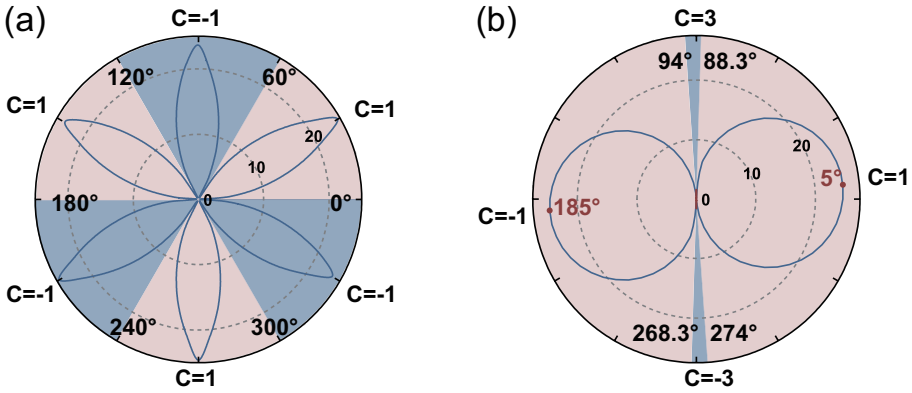

Fig. S9 For Ti_2P_2, **(a)** phase diagram of Chern number as a function of azimuthal angle φ for in-plane magnetization, and **(b)** phase diagram of Chern number as a function of polar angle θ for the out-of-plane magnetization along $\varphi = 30^\circ$ path.

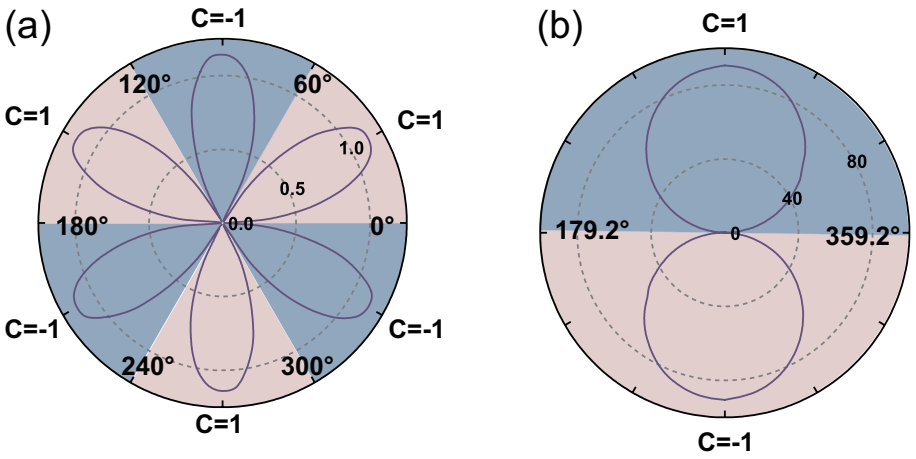

Fig. S10 For Ti_2Bi_2, **(a)** the phase diagram of Chern number as a function of azimuthal angle φ for in-plane magnetization, and **(b)** the phase diagram of Chern number as a function of polar angle θ for the out-of-plane magnetization along $\varphi = 30^\circ$ path.

References

1. G. Kresse and D. Joubert, From ultrasoft pseudopotentials to the projector augmented-wave method, *Phys. Rev. B* 59(3), 1758(1999)
2. G. Kresse and J. Hafner, *Ab initio* molecular dynamics for liquid metals, *Phys. Rev. B* 47(1), 558(1993)
3. J. P. Perdew, K. Burke, and M. Ernzerhof, Generalized Gradient Approximation Made Simple, *Phys. Rev. Lett.* 77(18), 3865(1996)
4. A. Togo, F. Oba, and I. Tanaka, First-principles calculations of the ferroelastic transition between rutile-type and $CaCl_2$-type SiO_2 at high pressures, *Phys. Rev. B* 78(13), 134106(2008)
5. G. Pizzi, V. Vitale, R. Arita, S. Blügel, F. Freimuth, G. Géranton, M. Gibertini, D. Gresch, C. Johnson, T. Koretsune, J. Ibañez-Azpiroz, H. Lee, J.-M. Lihm, D. Marchand, A. Marrazzo, Y. Mokrousov, J. I. Mustafa, Y. Nohara, Y. Nomura, L. Paulatto, S. Poncé, T. Ponweiser, J. Qiao, F. Thöle, S. S. Tsirkin, M. Wierzbowska, N. Marzari, D. Vanderbilt, I. Souza, A. A. Mostofi, and J. R. Yates, Wannier90 as a community code: new features and applications, *J. Phys.: Condens. Matter* 32(16), 165902(2020)
6. Q. Wu, S. Zhang, H. F. Song, M. Troyer, and A. A. Soluyanov, WannierTools: An open-source software package for novel topological materials, *Comput. Phys. Commun.* 224, 405(2018)